# PCCP

Accepted Manuscript


This is an *Accepted Manuscript*, which has been through the Royal Society of Chemistry peer review process and has been accepted for publication.

*Accepted Manuscripts* are published online shortly after acceptance, before technical editing, formatting and proof reading. Using this free service, authors can make their results available to the community, in citable form, before we publish the edited article. We will replace this *Accepted Manuscript* with the edited and formatted *Advance Article* as soon as it is available.

You can find more information about *Accepted Manuscripts* in the Information for Authors.

Please note that technical editing may introduce minor changes to the text and/or graphics, which may alter content. The journal's standard Terms & Conditions and the Ethical guidelines still apply. In no event shall the Royal Society of Chemistry be held responsible for any errors or omissions in this *Accepted Manuscript* or any consequences arising from the use of any information it contains.

ROYAL SOCIETY OF CHEMISTRY

www.rsc.org/pccp

Journal Name RSCPublishing

ARTICLE

# Lead-Iodide Nanowire Perovskite with Methylviologen Showing Interfacial Charge-Transfer Absorption: A DFT Analysis

Cite this: DOI: 10.1039/x0xx00000x

Received 00th January 2012,
Accepted 00th January 2012

DOI: 10.1039/x0xx00000x

www.rsc.org/

Jun-ichi Fujisawa*[ab] and Giacomo Giorgi[c]

Methylviologen lead-iodide perovskite ($MVPb_2I_6$) is a self-assembled one-dimensional (1-D) material consisting of lead-iodide nanowires and intervening organic electron-accepting molecules, methylviologen ($MV^{2+}$). $MVPb_2I_6$ characteristically shows optical interfacial charge-transfer (ICT) transitions from the lead-iodide nanowire to $MV^{2+}$ in the visible region and unique ambipolar photoconductivity, in which electrons are transported through the three-dimensional (3-D) organic network and holes along the 1-D lead-iodide nanowire. In this paper, we theoretically study the electronic band-structure of $MVPb_2I_6$ by density functional theory (DFT) calculations. Our results clearly confirm the experimentally reported type-II band alignment, whose valence band mainly consists of *5p* (I) orbitals of the lead-iodide nanowires and conduction band of the lowest unoccupied molecular orbital of $MV^{2+}$. The DFT calculation reveals weak charge-transfer interactions between the lead-iodide nanowires and $MV^{2+}$. In addition, the electronic distributions of the valence and conduction bands indicate the 3-D transport of electrons and 1-D transport of holes, supporting the reported experimental result.

## Introduction

Organic-inorganic metal-halide perovskites are self-assembled hybrid materials, which consist of anionic metal-halide inorganic semiconductive frameworks and charge-compensating organic cations.[1-3] For the organic-inorganic hybrid perovskites, the dimensionality of the inorganic framework can be controlled by the kind of organic cations from 0 (dot) to 1 (wire), 2 (well) and 3 (bulk).[1-3] The optical and conductive properties of these perovskites have been studied extensively.[1-3] Photoconductive properties of the perovskites was reported in 2005 for one-dimensional (1-D) lead-iodide nanowire perovskite ($MVPb_2I_6$) with methylviologen ($MV^{2+}$).[4] In 2009, Miyasaka's group first developed $TiO_2$-based electrochemical photovoltaic cells sensitized by three-dimensional (3-D) methylammonium lead-halides ($MAPbX_3$, X: Br, I).[5] Since then, efficient perovskite solar cells with 3-D $MAPbX_3$ have been rapidly developed by Park's, Snaith's and Gratzel's groups.[6-9] For the 3-D perovskites, their light-absorption and photoconductive properties are governed by the 3-D inorganic semiconducting framework.[10-13] On the other hand, the mentioned 1-D $MVPb_2I_6$ nanowire perovskite has intriguing optical and photoconductive properties, in which both the organic and inorganic components take part.[4,14,15]

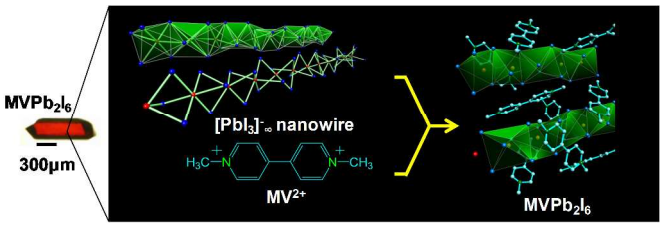


Figure 1. Photograph of a single crystal of $MVPb_2I_6$ with back-side illumination and crystal structure.

As shown in Figure 1, the 1-D $MVPb_2I_6$ perovskite is a unique nanowire material that consists of ultrathin face-sharing lead-iodide chains ($[PbI_3]^-_\infty$) with a diameter of ca. 0.5 nm and intervening organic electron-accepting $MV^{2+}$ molecules.[16] $MVPb_2I_6$ shows a dark red crystal colour, although the inorganic nanowire and $MV^{2+}$ have wide optical-gaps higher than 3.5 eV[17-19]. This dark-red coloration of $MVPb_2I_6$ results from the optical interfacial charge-transfer (ICT) transitions (so-called spatially indirect transitions) from the valence band of the lead-iodide nanowire to the unoccupied molecular orbitals of $MV^{2+}$, as shown in Figure 2(a).[4,14,15] With the ICT transitions, $MVPb_2I_6$ shows a broad absorption band in the

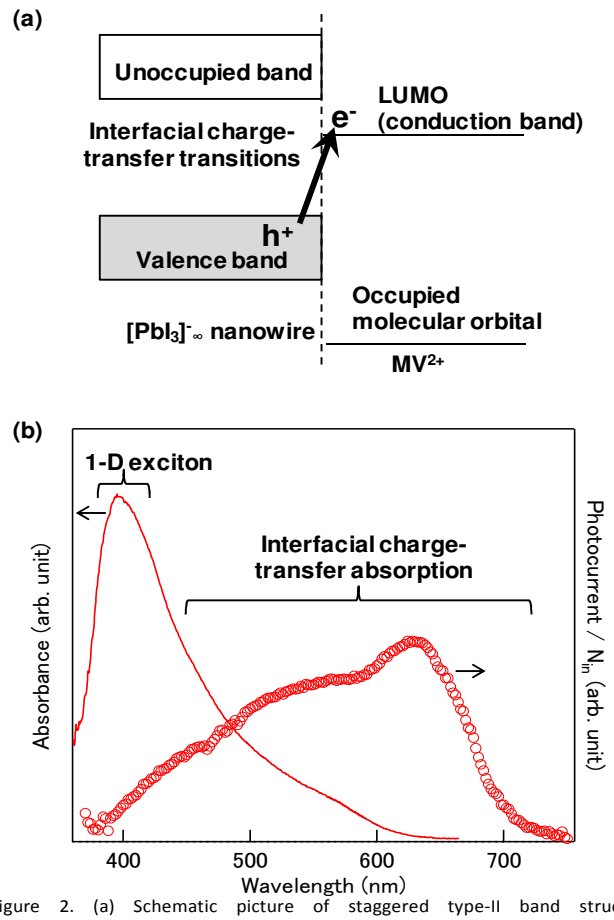


Figure 2. (a) Schematic picture of staggered type-II band structure experimentally deduced for $MVPb_2I_6$ and (b) Near UV-visible absorption spectrum of a cleaved crystal of $MVPb_2I_6$ (red curve) and the excitation spectrum of photocurrent divided with incident photon number ($N_{in}$) for $MVPb_2I_6$ (red circles). The experimental data were reported in Refs. 4 and 14.

visible region in addition to a 1-D exciton absorption at 400 nm, as shown in Figure 2(b). The ICT transitions induce photocurrent much more efficiently as compared to the 1-D exciton absorption.[4,14] In addition, the measurement of the anisotropy in the photoconductivity suggested ambipolar photocarrier transport, in which photogenerated electrons are transported three-dimensionally through the organic network and holes one-dimensionally in the nanowire.[4] Unfortunately, conclusive results concerning the staggered band structure (so-called type-II band alignment, see Figure 2(a)) and electronic properties of photocarriers are not available yet. In this paper, we theoretically study the electronic band structure of $MVPb_2I_6$ by density functional theory (DFT) calculations and discuss the photocarrier properties.

## Computational details

Both a periodic and a cluster approach have been employed in our research. Concerning the former, DFT calculations of the band structure of $MVPb_2I_6$ have been performed with the generalized gradient approximation as implemented in the VASP code[20,21] by means of the electron exchange-correlation functional proposed by Perdew-Burke-Ernzerhof (PBE)[22]. The electron-ion interaction is described by the projector augmented wave method (PAW)[23,24]. Also, still concerning the PAW potential, a $5d^{10}6s^26p^2$ valence electron potential was used for Pb atom. The plane-wave basis set energy cut-off was 500 eV. For the structural optimization, a 2x2x2 $\Gamma$-centered $k$-point sampling of the Brillouin Zone was used, while for the study of electronic properties denser meshes have been used (30 $k$-points). Due to the presence of heavy elements, relativistic effects are taken into account in the calculation of the electronic properties of $MVPb_2I_6$. Recent papers concerning Pb-based perovskite bulk systems have shown how the inclusion of spin-orbit coupling (SOC) effects becomes mandatory in order to obtain an improved description of such properties[12,13]. Additionally, preliminary calculations based on meta-GGA functionals have been performed. In detail the RTPSS functional[25] has been used without the inclusion of relativistic effects. We are aware that the modified Becke & Johnson (MBJ) potential[26,27] in principle yields band gaps with an accuracy very close to that of hybrid functional or GW methods, at the same time it is well-documented that the same potential tends to diverge (as we found in our calculations) in the case of low-dimensional systems. For this reason after a careful testing procedure we did not consider MBJ potential in our calculations. We remind that meta-GGA calculations require pseudo-potentials including information on the kinetic energy density of the core-electrons; thus in this last case a slightly different set (compared with calculations at DFT+SOC level) of pseudo-potentials were used. Negligible differences were found by the comparison of the results obtained with the two sets employed at the initial DFT level.

The experimental rhombohedral crystal structure reported by Tang et al.[16] ($R$-3, $Z$=3) was used and kept frozen in the calculations. Since no hydrogen coordinates of $MV^{2+}$ have been reported in their paper, the C-H bonds were optimized by DFT. Since $MVPb_2I_6$ includes heavy Pb and I atoms, spin-orbit couplings of all the atoms were taken into account. At cluster level, DFT calculations of $MV^{2+}$ and piperidinium ions ($PD^+$) were carried with the PBEPBE[22] functional and 6-31G+(d,p)[28,29] basis set using Gaussian 09 software[30]. As reported by Matteo, for $MV^{2+}$, a slightly twisted structure about the inter-ring C-C bond is the most stable.[31] However, since $MV^{2+}$ in $MVPb_2I_6$ has a planar form, our calculation was carried out with the restriction that the two methylpyridinium rings are coplanar. We confirmed that similar calculation results are obtained with other functionals such as B3LYP[32,33].

## Results and discussion

Figures 3(a) and 3(b) show the DFT+SOC calculated band structure and density of states (DOS) of $MVPb_2I_6$, respectively. From these figures, we can see that the valence band mainly consists of the $5p$ (I) orbitals with a very minor contribution of the $6s$ (Pb) orbitals of the lead-iodide nanowires. Accordingly, the valence band is localized in the lead-iodide nanowires, as

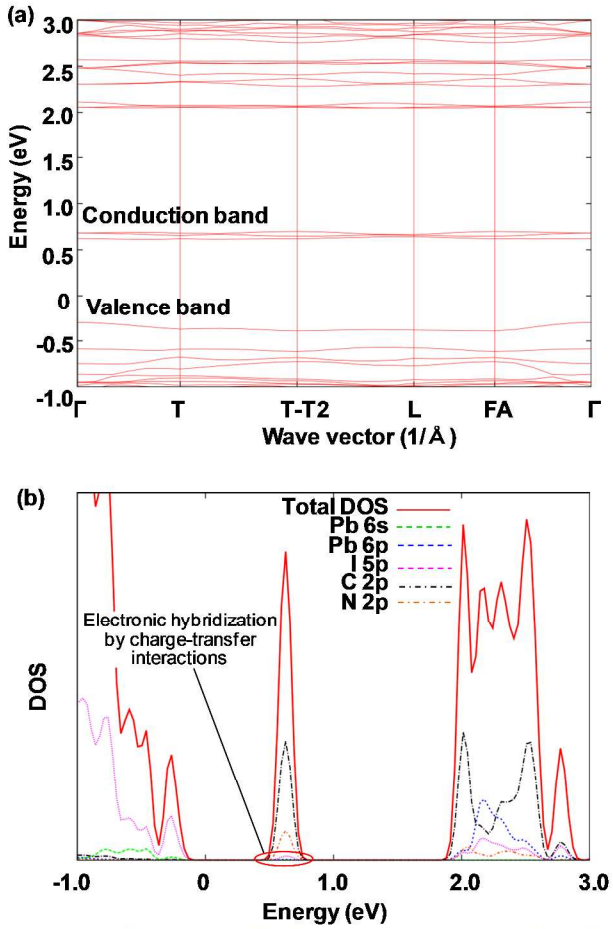


Figure 3. (a) Band structure and (b) density of states (DOS) of $MVPb_2I_6$ calculated by DFT including spin-orbit coupling effects.

shown in Figure 4(a). On the other hand, the conduction band in $MVPb_2I_6$ is located ca. 0.8 eV above the valence band. The conduction band consists of *2p* (C) and *2p* (N) orbitals of the $MV^{2+}$ molecules. In consequence, in contrast to the valence band, the conduction band of $MVPb_2I_6$ is localized on the $MV^{2+}$ molecules, as shown in Figure 4(b). Therefore, the valence and conduction bands in $MVPb_2I_6$ are spatially separated in the inorganic and organic moieties, respectively. Thus, the DFT+SOC calculation reveals the experimentally reported staggered band alignment (Figure 2(a)). However, the band gap (ca. 0.8 eV) of $MVPb_2I_6$ is quite underestimated as compared to the absorption onset energy (2.15-2.16 eV)[4] of the ICT band. Such underestimation is considered to be a typical shortcoming of DFT calculations.[12,13] On the other hand, we found that the conduction band is weakly hybridized with the *5p* orbitals of the I atoms. In addition, the DFT calculation suggests higher-energy unoccupied bands significantly delocalized on both the $MV^{2+}$ molecules and lead-iodide nanowires. Calculations by means of meta-GGA functional[25] (as stated without SOC effects) significantly improved the band gap up to 1.66 eV, without altering the band-edge properties.

We compare the electronic structure of $MVPb_2I_6$ with that of the 1-D $PDPbI_3$ perovskite reported by Azuma et al.[34]

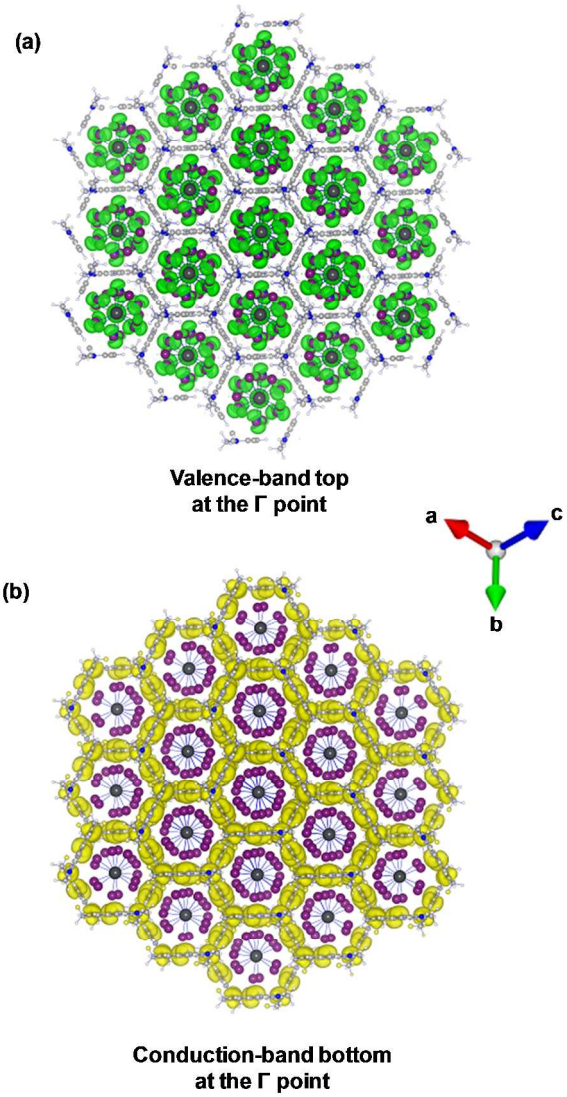


Figure 4. Isosurface plots of electron-density distributions of (a) the top of the valence band and (b) the bottom of the conduction band in $MVPb_2I_6$. (isovalue = 0.0001). Large dark gray: lead, purple: iodine, small gray: carbon, blue: nitrogen, white: hydrogen atoms.

$PDPbI_3$ consists of similar lead-iodide nanowires to those in $MVPb_2I_6$ and piperidinium cations ($PD^+$) instead of $MV^{2+}$. For $PDPbI_3$, both the valence and conduction bands are localized in the lead-iodide nanowires, indicating a type-I band alignment. The atomic-orbital component of the valence band in $MVPb_2I_6$ almost agrees with that in $PDPbI_3$. Therefore, the difference in the electronic structure between $MVPb_2I_6$ (type-II) and $PDPbI_3$ (type-I) is considered to be due to the difference in electronic properties between $MV^{2+}$ and $PD^+$.

Figure 5 shows the DFT calculated energy-level diagram of the highest occupied molecular orbital (HOMO) and the lowest unoccupied molecular orbital (LUMO) of $MV^{2+}$ and $PD^+$ in vacuum. The DFT calculations revealed that the LUMO of $MV^{2+}$ is much lower in energy by 5.8 eV than that of $PD^+$. The deeper LUMO level is consistent with the electron-accepting

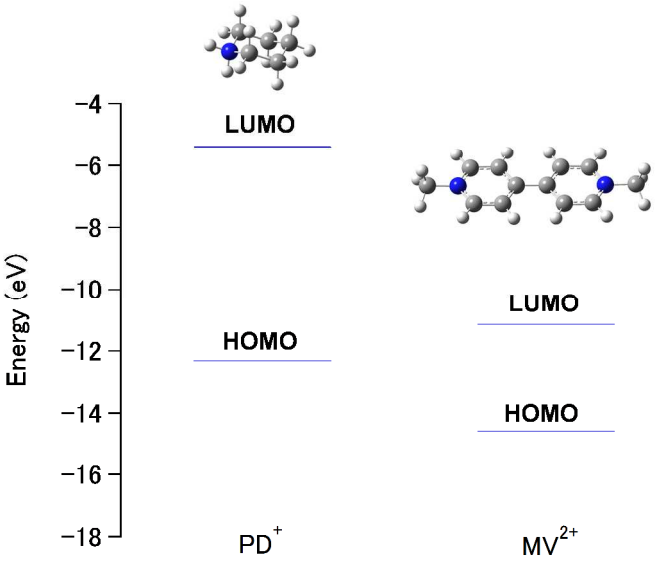


Figure 5. Energy-level diagram of HOMO and LUMO of $PD^+$ and $MV^{2+}$ calculated by DFT together with optimized structures of $PD^+$ and $MV^{2+}$. Gray: carbon, blue: nitrogen, white: hydrogen atoms.

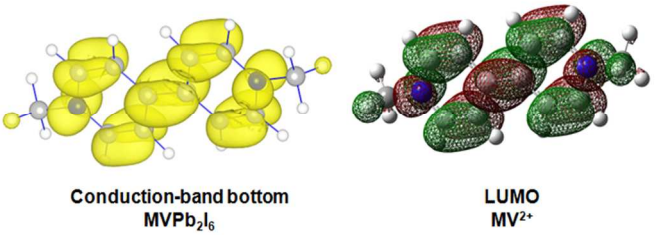


Figure 6. Isosurface plots of electron-density distribution (yellow isosurface, isovalue = 0.0001) of the conduction-band bottom on $MV^{2+}$ and electronic distribution (green and brown isosurfaces, isovalue = 0.02) of LUMO of $MV^{2+}$. Gray: carbon, blue: nitrogen, white: hydrogen atoms.

property of $MV^{2+}$. We compare the electron-density distribution of the conduction-band bottom with the electronic distribution of the LUMO in $MV^{2+}$. As shown in Figure 6, it can be seen that the conduction band of $MVPb_2I_6$ consists of the LUMO of $MV^{2+}$. Therefore, the difference in the band structure between $PDPbI_3$ (type-I) and $MVPb_2I_6$ (type-II) is attributed to the difference in the energy of the LUMO level between $MV^{2+}$ and $PD^+$.

As mentioned above, the conduction band localized on $MV^{2+}$ is weakly hybridized with the *5p* orbitals of I atoms in the lead-iodide nanowires, as shown in Figure 3. Since the valence band is predominantly comprised of the *5p* orbitals, the electronic hybridization is considered to result from weak charge-transfer interactions between the valence band located in the lead-iodide nanowires and LUMO of $MV^{2+}$. In the previous paper, we deduced the existence of the charge-transfer interaction between the lead-iodide nanowire and $MV^{2+}$ from the vibrational structure measured by FT-IR.[15] The calculation result supports the deduction.

Here, we discuss the properties of the photocarrier transports in $MVPb_2I_6$ on the basis of the calculation results. At first, as shown in Figure 3, the band widths of the conduction

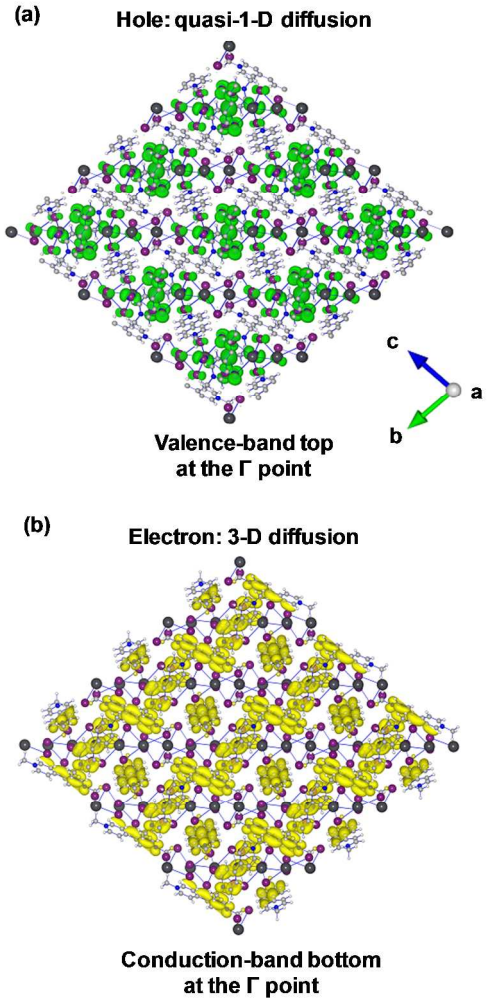


Figure 7. Electron-density distributions of (a) the valence-band top (green isosurface, isovalue = 0.0001) and (b) conduction-band bottom (yellow isosurface, isovalue = 0.0001) viewed along the *a* axis.

and valence bands are estimated to be less than ca. 0.3 eV. The narrow band widths imply the polaron formation of the photogenerated electrons and holes with the strong electron-lattice interactions in $MVPb_2I_6$.[4] Fujisawa *et al.* examined the electron-lattice interaction in $MVPb_2I_6$ from the analysis of the absorption tail of the ICT band with Urbach's equation ($A=A_0\exp(\sigma\beta(E - E_0))$, $\sigma$: steepness constant).[4] The obtained steepness constant of 0.35 is quite small as compared to those (0.6–3) for other inorganic semiconductors and insulators.[35] This result indicates that the electron-lattice coupling in $MVPb_2I_6$ is quite strong. Thus, because of the narrow band widths of the conduction and valence bands and strong electron-lattice interaction, photogenerated electrons and holes are considered to relax to polarons. The polaron formation is consistent with the reported observation of the photoluminescence from spatially-separated polaron-pairs in $MVPb_2I_6$.[14]

The measurement of the anisotropy in the photoconductivity in $MVPb_2I_6$ indicated ambipolar photocarrier transport, in which photogenerated holes are transported one-

dimensionally in the nanowire and electrons three-dimensionally through the organic network.[4] Figure 7 shows the electron-density distributions of the valence and conduction bands viewed along the *a* axis. Since the inter-wire electronic coupling is quite weak as compared to the intra-wire one, as shown in Figure 7(a), photogenerated hole-polarons are predominantly transported along the nanowire. On the other hand, photogenerated electron-polarons are considered to be transported by thermally-activated hoping through the 3-D organic network, since there are little electronic overlaps between neighbouring molecules, as shown in Figure 7(b). Therefore, the calculation result is consistent with the ambipolar transport.[4]

## Conclusion

We theoretically clarified the electronic band-structure of $MVPb_2I_6$ by the DFT calculations. DFT calculations reveal the experimentally reported type-II band alignment, in which the conduction band is localized on the $MV^{2+}$ molecules and valence band in the lead-iodide nanowires. The DFT calculation reveals electronic hybridization between the conduction band on $MV^{2+}$ and the valence band in the nanowires by charge-transfer interactions. The narrow band widths (< 0.3 eV) of the conduction and valence bands suggest the polaron formation of the photogenerated electrons and holes. In addition, the electronic distributions of the conduction and valence bands indicate the 3-D electron and 1-D hole transports, which are consistent with the reported experimental result.

## Acknowledgements

This research was supported by the Precursory Research for Embryonic Science and Technology (PRESTO) program of the Japan Science and Technology Agency (JST). The author (G.G.) thanks Prof. Koichi Yamashita of the University of Tokyo for supporting the analysis of electronic properties of the material and for the always fruitful and stimulating scientific discussions.

## Notes and references

[a]Research Center for Advanced Science and Technology (RCAST), The University of Tokyo, 4-6-1 Komaba, Meguro-ku, Tokyo 153-8904, Japan. E-mail: ufujisw@mail.ecc.u-tokyo.ac.jp
[b]Japan Science and Technology Agency (JST), Precursory Research for Embryonic Science and Technology (PRESTO), 4-1-8 Honcho Kawaguchi, Saitama 332-0012, Japan.
[c]Department of Chemical System Engineering, School of Engineering, The University of Tokyo, 7-3-1, Hongo, Bunkyo-ku, Tokyo 113-8656, Japan.

1. T. Ishihara, *Optical Properties of Low-Dimensional Materials*, edited by T. Ogawa and Y. Kanemitsu Ch. 6, World Scientific, Singapore, 1995.
2. G. C. Papavassiliou, *Prog. Solid St. Chem.*, 1997, **25**, 125.
3. D. B. Mitzi, *Prog. Inorg. Chem.*, 1999, **48**, 121.
4. J. Fujisawa and N. Tajima, *Phys. Rev. B*, 2005, **72**, 125201.
5. A. Kojima, K. Teshima, Y. Shirai and T. Miyasaka, *J. Am. Chem. Soc.*, 2009, **131**, 6050.
6. H.-S. Kim, C.-R. Lee, J.-H. Im, K.-B. Lee, T. Moehl, A. Marchioro, S.-J. Moon, R. Humphry-Baker, J.-H. Yum, J. E. Moser, M. Grätzel and N.-G. Park, *Scientific Rep.*, 2012, **2**, 591.
7. M. M. Lee, J. Teuscher, T. Miyasaka, T. N. Murakami and H. J. Snaith, *Science*, 2012, **338**, 643.
8. J. Burschka, N. Pellet, S.-J. Moon, R. Humphry-Baker, P. Gao, M. K. Nazeeruddin and M. Grätzel, *Nature*, 2013, **499**, 316.
9. M. Liu, M. B. Johnston, H. J. Snaith, *Nature*, 2013, **501**, 395.
10. T. Umebayashi, K. Asai, T. Kondo and A. Nakao, *Phys Rev B*, 2003, **67**, 155405.
11. E. Mosconi, A. Amat, M. K. Nazeeruddin, M. Grätzel and F. D. Angelis, *J. Phys. Chem. C*, 2013, **117**, 13902.
12. J. Even, L. Pedesseau, J.-M. Jancu and C. Katan, *J. Phys. Chem. Lett.*, 2013, **4**, 2999.
13. G. Giorgi, J. Fujisawa, H. Segawa and K. Yamashita, *J. Phys. Chem. Lett.*, 2013, **4**, 4213.
14. J. Fujisawa and T. Ishihara, *Phys. Rev. B*, 2004, **70**, 113203.
15. J. Fujisawa, N. Tajima, K. Tamaki, M. Shimomura and T. Ishihara, *J. Phys. Chem. C*, 2007, **111**, 1146.
16. Z. Tang and A. Guloy, *J. Am. Chem. Soc.*, 1999, **121**, 452.
17. A. Nagami, K. Okamura and T. Ishihara, *Physica B*, 1996, **227**, 346.
18. T. Fukumoto, M. Hirasawa and T. Ishihara, *J. Lumin.*, 2000, 87-89, 497.
19. M. Mohammad, *J. Org. Chem*., 1987, **52**, 2779.
20. G. Kresse and J. Furthmüller, *Comput. Mater. Sci.*, 1996, **6**, 15.
21. G. Kresse and J. Furthmüller, *Phys. Rev. B*, 1996, **54**, 11169.
22. J. P. Perdew, K. Burke, M. Ernzerhof, *Phys. Rev. Lett.* 1996, 77, 3865.
23. P. E. Blöchl, *Phys. Rev. B*, 1994, **50**, 17953.
24. G. Kresse and D. Joubert, *Phys. Rev. B*, 1999, **59**, 1758.
25. J. Sun, M. Marsman, G. I. Csonka, A. Ruzsinszky, P Hao, Y.-S. Kim, G. Kresse, and J. P. Perdew, *Phys. Rev. B* , 2011, **84**, 035117.
26. A. D. Becke and E. R. Johnson, *J. Chem. Phys.* 2006, **124**, 221101.
27. F. Tran and P. Blaha, *Phys. Rev. Lett.,* 2009, **102**, 226401.
28. R. Ditchfield, W. Hehre and J. Pople, *J. Chem. Phys.*, 1971, **54**, 724.
29. W. Hehre, R. Ditchfield and J. Pople, *J. Chem. Phys.*, 1972, **56**, 2257.
30. M. J. Frisch, *at al.* Gaussian 09, Revision D.01, Gaussian, Inc., Wallingford, CT, 2009.
31. A. di Matteo, *Chem. Phys. Lett.* **2007**, 439, 190–198.
32. A.D. Becke, *J. Chem. Phys.*, 1993, **98**, 5648.
33. C. Lee, W. Yang and R. G. Parr, *Phys. Rev. B*, 1988, **37**, 785.
34. J. Azuma, K. Tanaka, M. Kamada and K. Kan'no, *J. Phys. Soc. Jpn.* **2002**, 71, 2730.
35. M. Ueta, H. Kanzaki, K. Kobayashi, Y. Toyozawa and E. Hanamura, *Excitonic Processes in Solids*, Springer-Verlag, Tokyo, 1984.